Investigation on characteristics of tensile damage and microstructure evolution of steel AISI 316L by nonlinear ultrasonic Lamb wave

Jianxun Li[1,2], Minghang Wang[1], Haofeng Chen[2,3] *, Pengfei Wang[4] *, Weiqiang Wang[1,5] *

1. Engineering and Technology Research Center for Special Equipment Safety of Shandong Province, Key Laboratory of High-efficiency and Clean Mechanical Manufacture (Ministry of Education), National Demonstration Center for Experimental Mechanical Engineering Education (Shandong University), School of Mechanical Engineering, Shandong University, 17923 Jing Shi Road, Jinan 250061, China

2. Department of Mechanical and Aerospace Engineering, University of Strathclyde, Glasgow G1 1XJ, UK

3. Key Laboratory of Pressure Systems and Safety, School of Mechanical and Power Engineering, East China University of Science and Technology, Shanghai, 200237, China

4. Institute of Process Equipment and Control Engineering, School of Mechanical Engineering, Zhejiang University of Technology, Hangzhou 310023, China

5. College of Electromechanical Engineering, Qingdao University of Science and Technology, Qingdao, 266061, China

** Corresponding author. Tel.: +86-531-8839-5100; fax: +86-531-8839-5100.*

E-mail address: sduefascf@163.com (Weiqiang Wang), pfwang@zjut.edu.cn (Pengfei Wang) haofeng.chen@strath.ac.uk (Haofeng Chen)

Abstract: In view of the high sensitivity to microstructure evolution of higher harmonics generated by the nonlinear ultrasonic method, the tensile damage in the stainless steel AISI 316L was evaluated by nonlinear ultrasonic Lamb wave. The effect of different degree of tensile deformation on nonlinear ultrasonic response in 316L was analyzed by considering the microstructure evolution and the test results. First, the power-law relation of nonlinear ultrasonic parameter and plastic strain is proposed. Meanwhile, martensitic transformation and the increasing of dislocation density can be observed in the micrographs of specimens with the increase of plastic deformation. Then, the same variation tendency of intergranularly averaged Kernel Average Misorientation（KAM , as well as the relative nonlinear ultrasonic parameter, demonstrated that the nonlinearity due to tensile damage is controlled by the evolution of microstructure that directly affects higher order elastic constant of stainless steel 316L. Furthermore, based on continuous damage mechanics, the method quantitatively characterizes the degradation of mechanical properties was proposed with a functional relation of damage variable and relative nonlinear parameter. The method proposed in this study provides a theoretical basis for online monitoring of the damage status of in-service equipment. It is of great significance for residual life assessment, structure integrity assessment, and service life extension of equipment.

Keywords: AISI 316L; Tensile damage; Nonlinear ultrasonic Lamb wave; Kernel Average Misorientation（KAM）

This is a peer reviewed, accepted author manuscript of the following research article: Li, J., Wang, M., Chen, H., Wang, P., & Wang, W. (2022). Investigation on characteristics of tensile damage and microstructure evolution of steel AISI 316L by nonlinear ultrasonic Lamb wave. *International Journal of Pressure Vessels and Piping*, 198, [104680]. https://doi.org/10.1016/j.ijpvp.2022.104680

1. Introduction

As a typical type of steels used in pressure vessels, austenitic stainless steels are widely employed in nuclear energy, petrochemical and other fields [1, 2]. It is inevitable to appear the different degrees of degradation on the damage and mechanical properties of the stainless steel components during the processing and service stages. Plastic damage caused by irreversible deformation due to the tensile or compressive stress exceeding the elastic limit of the components is the most common damage type in engineering practice, and it is also one of the essential reasons for the failure of engineering equipment. Effective characterization and evaluation of the state of plastic damage are, therefore, of great importance to ensure safe operation, predict the residual life, and promote life-extension of equipment.

Ultrasonic testing technology is widely adopted for assessing the damage in engineering components due to its unique advantages of wide applicability, convenient detection, and high reliability [3, 4]. A transmissibility-based processing method was proposed with the phased ultrasonic array A-scan data to identify and size the surface cracks in stainless pipes with circumferential welds [5]. Ben et al.[6] used the Lamb wave produced by ultrasonic pulse generator at a particular frequency dealing with the damage identification in composite materials without using any analytical models. They concluded that the ultrasonic methods using Lamb wave have the potential to provide more information than frequency response methods since their sensibility to the local effects of damage. For accurate and high-resolution reconstruction of the wall thickness loss in isotropic plates, Rao et al.[7] studied the guided wave tomography algorithms and introduced a method based on full waveform inversion. However, the above ultrasonic testing techniques based on the linear wave theory, which could detect the macro defects (inclusions, cracks, etc. with the measurement of the wave velocity, attenuation and scattering coefficient, are not available for the detecting the micro-nano scale defect since the evolution of microstructure cannot cause the change of the linear parameters [8] Once the macro defects appear on the service component, the cracks will propagate further if the external loading imposes continuously, which shows that the actual bearing capacity of the service component has been significantly weakened [9]. Therefore, effectively detecting and evaluating the early damage of materials in time has important practical significance.

There are many studies suggest that nonlinear ultrasonic technique has high sensitivity to the early microstructure evolution around the internal damage of metal components [10, 11]. The early damage of metallic materials is mainly due to the microstructure evolution at micro/nano scale, such as slip line enrichment, dislocation initiation and proliferation, cavity nucleation and growth at grain boundaries[12], etc. When the high-intensity ultrasonic wave input into the specimen and interacts with internal micro defects, the displacement and stress-strain relationship of the particle at the defect will change, resulting in the distortion of the ultrasonic waveform and the generation of high-order harmonic signals [10]. The detection mechanism and the generation of high-order harmonic are shown in Figure 1. Thus, the wave distortion has been considered for evaluating the microscopic damage since the value of the distortion intensity was depended on the variation of microstructure. The quantitative measurement of this wave distortion is given by nonlinear ultrasonic parameter β [13], as shown in Eq.(1

$$\beta = \frac{8}{k^2 x}\frac{A_2}{A_1^2} \qquad (1$$

where k is the wavenumber, x is the propagation distance. A_1, A_2 are the amplitudes of the fundamental and the second harmonic, respectively.

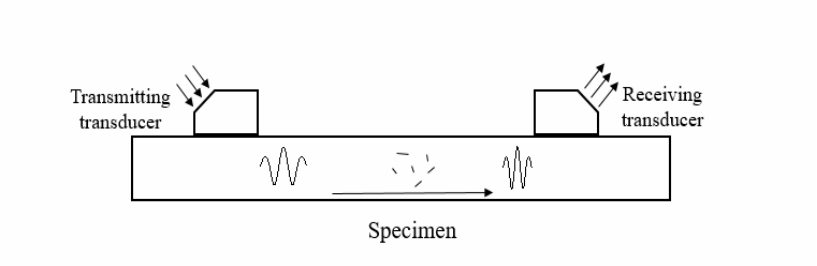

Figure 1. High-order harmonic generation

There is a lot of growing interest in detecting and evaluating the early plastic damage of metal components with the nonlinear ultrasonic wave. Herrmann et al. [14] studied the acoustic nonlinearity of Ni-based alloy experienced plastic deformation with Rayleigh wave. They found that the acoustic nonlinearity increased significantly in the initial plastic deformation stage. In another work, the tensile damage of the mild steel was investigated with nonlinear longitudinal wave and linear wave[15]. It was found that the nonlinear parameters showed a general upward trend when the load was within the steel's tensile strength, while the longitudinal wave velocities and attenuation coefficient did not show an obvious regularity. Using the nonlinear Lamb wave, Pruell et al. [16] demonstrated that the nonlinear parameters increase with the plastic strain increase in aluminum alloy when the phase velocity matches the group velocity. A similar response that the nonlinear parameter varies with the plastic deformation was observed by Viswanath et al. [17] and Zhang et al. [18] on the common steel for pressure vessels. Their microstructure analysis of different deformed stainless steels showed that the increase of nonlinear parameter during deformation was related to dislocation density. Although all studies above show that the acoustic nonlinearity of metallic materials depend on the damage state and the microstructural characteristics, few studies focus on the relationship between the evolution state of microstructure and the ultrasonic nonlinearity during the damage process. Besides, the papers about using the nonlinear ultrasonic method to evaluate the mechanical properties of the components in service and predict the residual life are even rarer.

This study focuses on investigating the nonlinear ultrasonic response of plastically deformed stainless steel 316L. Meanwhile, this paper attempts to quantify the degradation of mechanical properties of the material during the process of tensile by establishing the relationship of the damage variable with the ultrasonic nonlinear parameter, which would be helpful for predicting the residual life of similar materials with nondestructive testing technology.

2. Experimental procedure

2.1 Specimen preparation

The typical steel for pressure vessel, AISI 316L, was used in this presented work. The chemical composition of each material tested by the Bruker Tasman Q4 spectrograph is provided in Table 1 with the corresponding standards [19]. According to Chinese standard [20], the specimen was machined into the flat dog-bone-shaped with a thickness of 4mm, gauge length of 80mm and total length of 260 mm. The specific dimensions are shown in Figure 2. In order to avoid the influence of residual stress generated in the process of specimens preparation on ultrasonic detection, all samples underwent the same heat treatment process to remove residual stress.

Table 1 Chemical composition of the materials (wt.%).

Material	C	Si	Mn	Mo	P	Cr	Ni	S
316L	0.021	0.0524	1.179	2.125	0.026	16.91	10.25	0.003
ASTM A959[19]	≤ 0.030	≤1.00	≤2.00	2.00 ~ 3.00	≤0.045	16.00 ~ 18.00	10.00 ~ 14.00	≤0.030

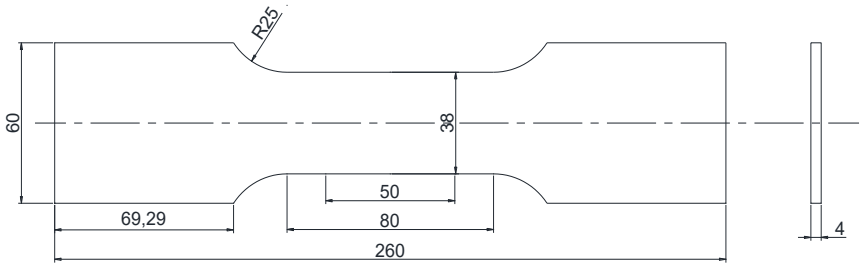

Figure 2. Dimension of flat dog-bone specimen (all dimensions are in mm .

2.2 Tensile tests

As shown in Figure 3, all tensile tests were performed on the ZwickRoell-Z250 with tensile rate of 1 mm/min. The monotonic tensile test for obtaining the mechanical property of the experimental materials and cyclic loading tensile tests (with 10 cycles and total strain of 50% for obtaining the damage variable of the material during the deformation were carried out. The tensile curves are shown in Figure 4, which can be seen the yield strength and tensile strength of the material were 271.3 MPa and 605.27 MPa, respectively. There is little difference between the material properties obtained by single tensile and cyclic tensile tests, so the subsequent analysis can match the damage degree of the cyclic tensile test with the sample under the same tensile degree.

For producing the tensile damage of different degrees, the interval tensile strain is divided into 7 times according to the strain value corresponding to tensile strength (5%-10%-15%-20%-25%-30%-40% . After each tensile test, the specimen shall be subjected to nonlinear ultrasonic test. Then, considering the effect of residual strain, the tensile test shall be carried out to the next strain value on the specimen. The necking stage is not considered in strain division, this is because only the relation between early damage caused by plastic deformation and nonlinear ultrasonic wave is studied in this paper.

Figure 3. The experimental equipment used in this study (ZwickRoell-Z250

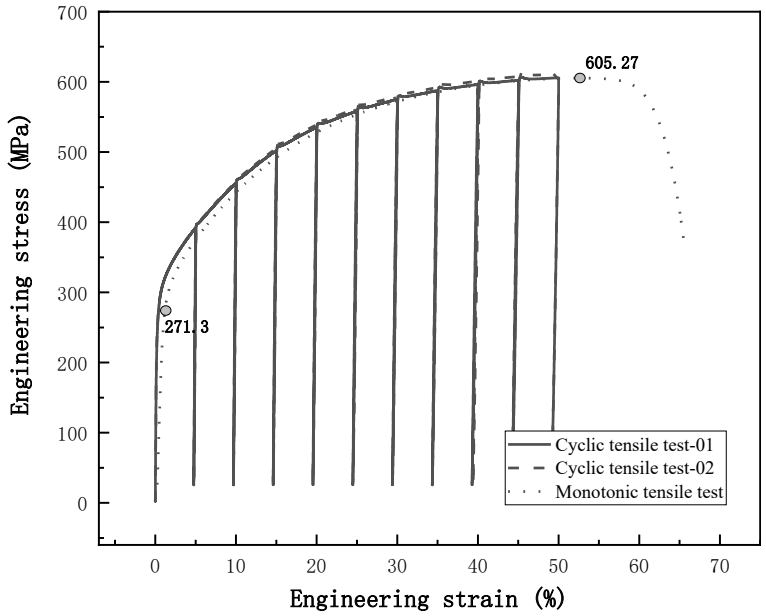

Figure 4. The stress-strain rupture curves and cyclic tensile curves of 316L

2.3 Nonlinear ultrasonic measurement

Figure 5(a and 5(c show the RITEC SNAP RAM-5000 high power ultrasonic system and the frame diagram of the Lamb wave-based nonlinear ultrasonic testing system. The system outputs a high-voltage tone burst signal of 20 cycles at the excitation frequency of 2.25 MPz, while a center frequency of 2.25 MHz piezoelectric transducer (Olympus V403 was used as the transmitter. The 5MHz piezoelectric transducer (Olympus V405 acted as the receiver for obtaining the fundamental wave and second harmonic components. Glycerol was used for coupling between transducer and wedge, also wedge and specimen（the oblique angle of the wedge is 27°[21]）, while using a customized fixed device (shown in Figure 5(b to give a constant pressure on the wedge for each measurement.

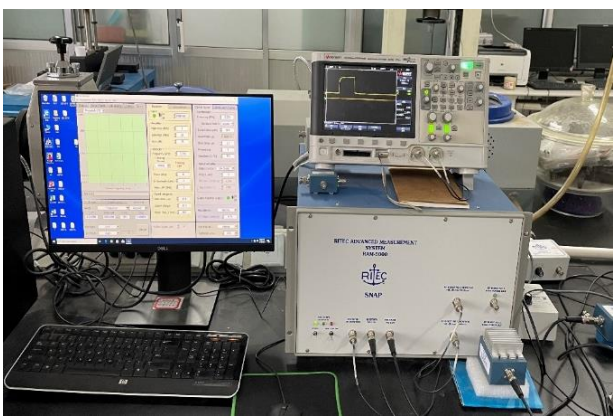

(a)

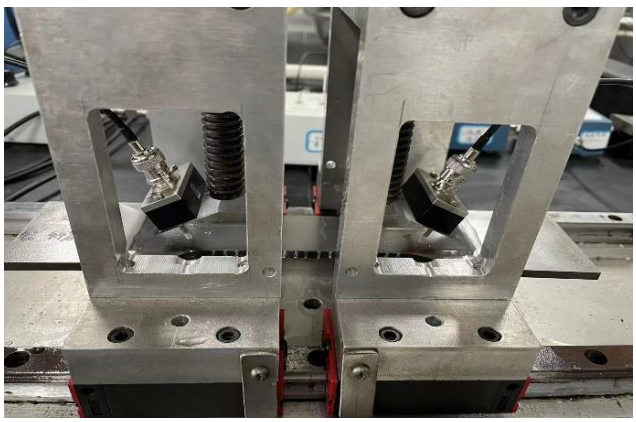

(b)

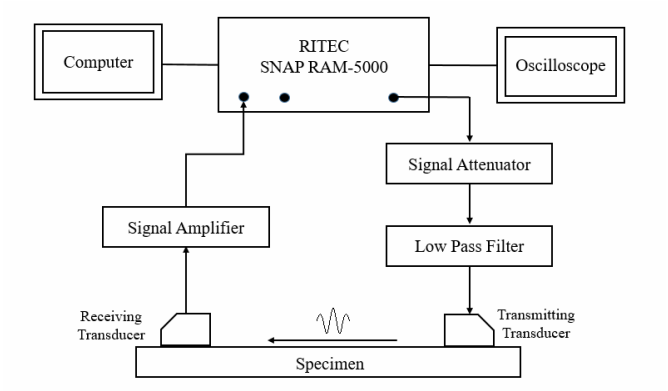

（c）

Figure 5. (a RITEC SNAP RAM-5000 high power ultrasonic system （b）Fixed device of the nonlinear ultrasonic testing (c Frame diagram of the Lamb wave-based nonlinear ultrasonic testing system

The phase velocity and group velocity dispersion curves of Lamb waves for the 4 mm thick stainless steel 316L, drawn by MATLAB 2014b, are shown in Figure 6. In order to excite the second harmonic of the Lamb wave as well as to avoid the separation of the harmonic packet and the fundamental packet in the propagation process, the phase velocity and the group velocity of the selected mode pair need to be matched [22]. Thus, the synchronous S2-S4 mode pair have been selected for higher harmonic measurement in this study.

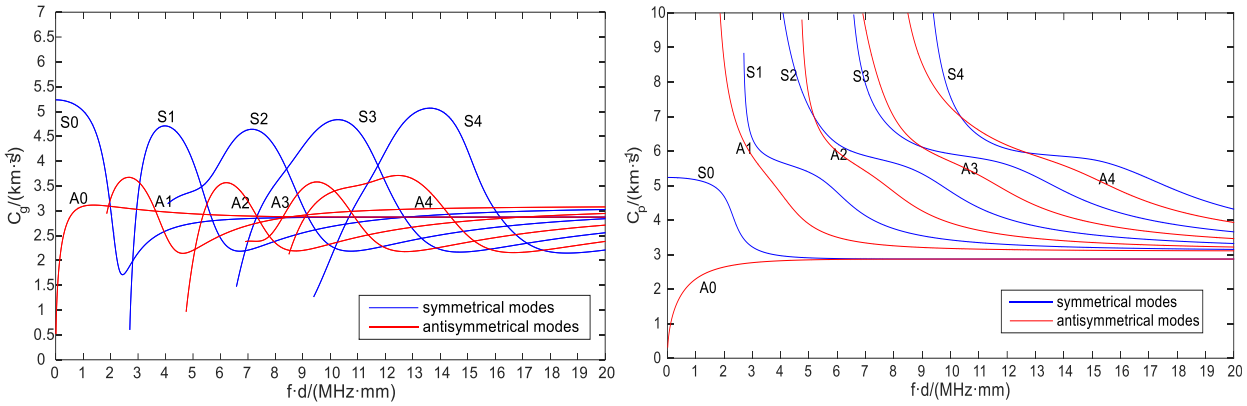

(a Group velocity curve (b Phase velocity curve

Figure 6. The dispersion curves of the 4mm thick 316L

As described in Eq.(1 , the wavenumber k is constant in the measurement while the wave propagation distance x (i.e., the test distance between transducers changes continuously with the tensile specimen under different degrees. It could be concluded that the ultrasonic nonlinear parameters $\beta \propto A_2/(xA_1^2)$. Therefore, the relative nonlinear parameter β' was defined as Eq.(2 .

$$\beta' = A_2 / (xA_1^2) \qquad (2$$

The normalized nonlinear parameter can be described as $(\beta'/\beta_0$, where β_0 is the nonlinear parameter of the original specimen. The linear increase of the normalized nonlinear parameter with x is presented in Figure 7, which indicates the cumulative effect of second harmonic and confirms that the material nonlinearity dominates the instrumental nonlinearity in this testing. To avoid wave overlap caused by short test distance and ensure no abrupt structure in the test section, the initial test distance is set as 80 mm. The subsequent tests were carried out at the marked position. For the reliability of the experimental results, each experiment was repeated 5 times.

Finally, the time domain signal measured during the testing was digitally processed and subjected to fast Fourier transform (FFT in order to obtain the amplitude of the fundamental frequency A_1 and second-harmonic frequency A_2. The normalized nonlinear parameter (β'/β_0 can be calculated with the Eq. (2 and β_0.

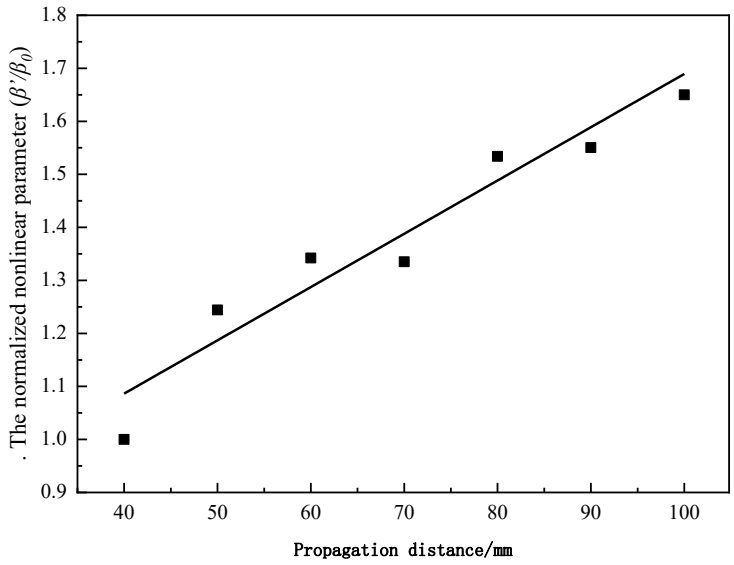

Figure 7. The relationship between the propagation distance and normalized nonlinear parameter

2.4 Observation of microstructures.

In order to characterize the damage evolution behavior of the 316L in the tensile process, TEM and SEM-EBSD observations were performed on samples cut from the center of the four tensile specimens with different plastic damage (0%, 10%, 20%, 40% .

The TEM specimens were polished to 100 micros thickness by electric spark cutting and mechanical polishing, and then were subjected to twinjet electro-polishing using 5% perchloric acid alcohol solution. The TEM observation was performed on Tecnai G2 F20 (FEI, USA at an electric voltage of 200 kV. According to the study [23], the dislocation density could be obtained from the TEM micrograph by drawing the grids. In this presented measurement, the grids consist of 4 horizontal lines and 4 vertical lines, and then the intersection of the dislocation line and each grid line is counted. Substituting the number of intersections into the following Eq.(3 [24], the dislocation density can be obtained.

$$\rho = \frac{1}{t}\left(\frac{\sum n_h}{\sum L_h} + \frac{\sum n_v}{\sum L_v}\right) \qquad (3$$

where t is the thickness of the foil (200nm in this study , n_h and n_v are the number of intersections on the horizontal line and vertical line, respectively, and L_h and L_v are the length of the horizontal line and vertical line, respectively.

All EBSD samples before observation were polished with 600#, 800# and 1200# sandpaper successively and then were polished with a solution containing 0.5um diamond particles for 30 minutes to remove scratches. The polished samples were subjected to normal temperature vibration corrosion polishing with 0.05um silica suspension on Buehler Automet polishing machine for 4-8 hours. The EBSD scanning was performed on ZEISS Sigma 300VP attached to Symmetry Scanning Electron Microscope at 70° tilting condition. An area of 300 × 300 μm was considered for EBSD scans for all the samples using a step size of 0.6 μm.

Two types of important intragranular misorientation parameters, KAM (Kernel Averaged Misorientation and GROD (Grain Reference Orientation Deviation , can be obtained by EBSD scan. KAM, defined as average misorientation between the measurement point and the surrounding adjacent points which belong to the same grain,

represents the orientation gradient at local points inside the grain. GROD is defined as the misorientation between the measurement point and its internal reference point of the grain and is used to characterize the degree of orientation inhomogeneity inside the grain. Figure 8, Eq. (4 and Eq. (5 show the definition of KAM and GROD which have been programmed into the post-processing software of EBSD and can be obtained directly [25]. The intragranular misorientation parameters have been widely used for grain distortion analysis and damage evaluation of the expiring metallic structural materials [26]. In addition, the intergranularly averaged KAM and GROD (i. e. $\overline{\mathrm{KAM}}$ and $\overline{\mathrm{GROD}}$, the average value of all grain in the observation area are proved in some studies that they show a good linear correlation with the macro uniaxial plastic deformation [27, 28].

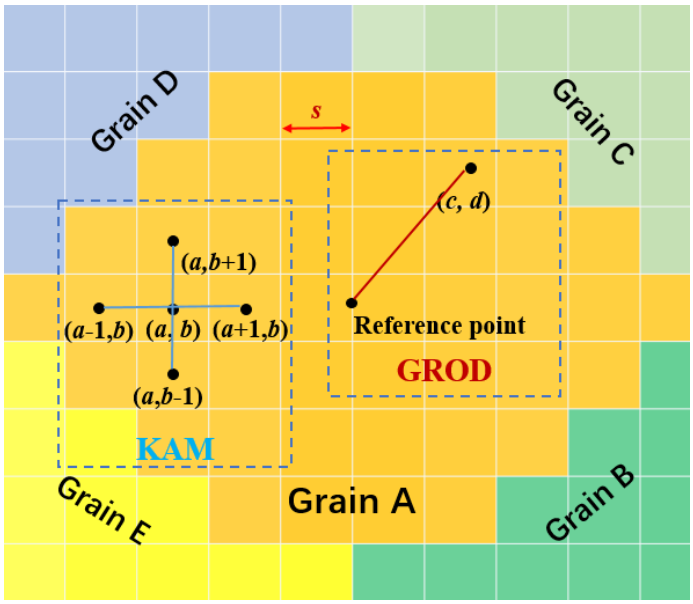

Figure 8. The definition of KAM and GROD [29].

$$\mathrm{KAM}(a,b)=\frac{1}{4}(\theta_{(a,b)}^{(a-1,b)}+\theta_{(a,b)}^{(a+1,b)}+\theta_{(a,b)}^{(a,b-1)}+\theta_{(a,b)}^{(a,b+1)}) \qquad (4$$

$$\mathrm{GROD}(c,d)=\theta_{ref}^{(c,d)} \qquad (5$$

where $\theta_{(a,b)}^{(a-1,b)}$ is the angle of misorientation between (a-1, b and (a, b .

3. Results and discussions

3.1 Characteristics of plastic deformation in nonlinear ultrasonic tests

The variation of the average value of β' (five measurements per point calculated by Eq.(2 with the plastic strain is plotted in Figure 9, which shows clearly that the relative nonlinear ultrasonic parameter increases with the increasing plastic strain. A power-law relation between β' and plastic strain obtained in this study, shown as the fitting line and the Eq.(6 , is basically consistent with the result presented by Viswanath et al.[17] in studying the AISI 304 stainless steel. It is seen that initially up to 20% plastic strain there is a slow increase in relative nonlinear parameter β' but started increasing rapidly from 20%, the β' for the 316L specimen with 40% plastic strain is about 3.2 times of that for the initial specimen.

$$\beta' = 5.848\times10^{-7}\varepsilon_p^2 - 3.008\times10^{-6}\varepsilon_p + 4.102\times10^{-4} \qquad (6$$

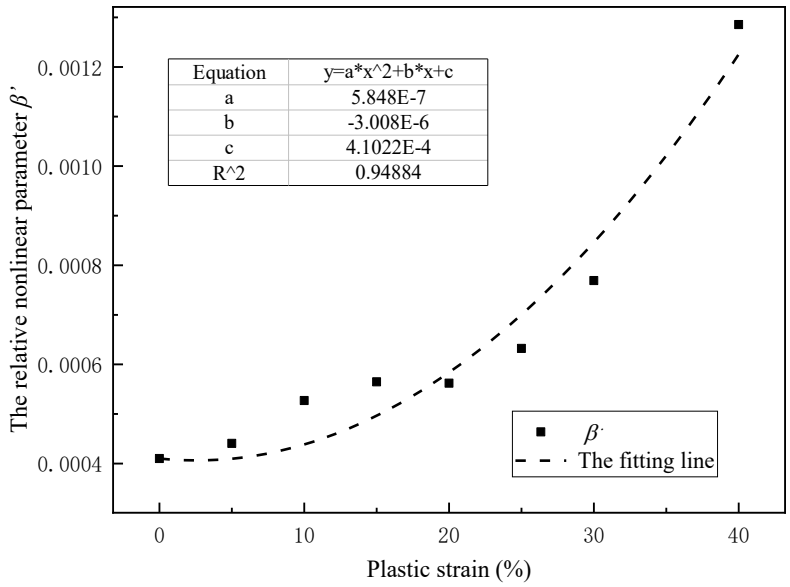

Figure 9. Variation of the relative nonlinear parameter β' with different plastic strain.

3.2 Mechanical properties of plastically deformed specimen

The true stress-strain curves of 316L from 10 cyclic loading and unloading tensile test are shown in Figure 10. The yield strength of samples with different degrees of deformation can be obtained from the engineering stress-strain curves in Figure 4, while Young's modulus E can be calculated from the unloading section of true stress-strain curves of each tensile test ($E=\sigma/\varepsilon$, only the first 40% data of unloading section was used to avoid the effect of back stress relaxation [30] and take the average of the two experimental value as the result). With that, the damage variable D of 316L, which can be calculated by Eq.(7) [31], is listed in Table 2.

$$D_i = 1 - \frac{E_i}{E_0} \tag{7}$$

where E_0 and E_i represent the Young's modulus of the original specimen and the specimen after ith tensile test, respectively.

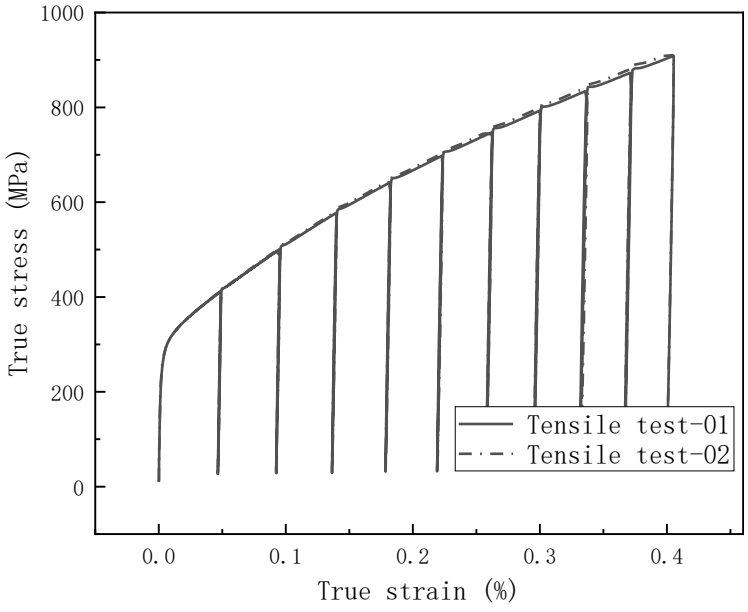

Figure 10 The true stress-strain curves of the 316L from 10 cyclic and unloading tensile test

From Table 2, the yield strength $\sigma_{0.2}$ of the material increases significantly with plastic strain. Combined with the metallographic observation shown in Figure 12, some changes in the microstructure of austenitic materials occur during the tensile process, which include the formation of martensitic phase transformation and the decreased grain particle size. It has been proved that lath martensite is a kind of high strength structure [32, 33]. The generation of phase transformation of the material changes the internal microstructure of grain and increases the resistance of dislocation movement, and then causes the yield strength of the specimen to increase continuously during plastic deformation with the grain refinement.

Table 2. Mechanical properties of 316L with various plastic strain

The *i*th tensile test	Plastic strain ε_p (%)	Yield strength $\sigma_{0.2}$ (MPa)	Young's modulus E_i (GPa)	Damage variable D_i
0	0	269.95	178.26	0
1	5	398.19	178.62	-0.002
2	10	462.1	174.69	0.02
3	15	508.42	171.35	0.039
4	20	540.65	170.02	0.046
5	25	563.36	169.37	0.05
6	30	579.51	166.37	0.067
7	35	591.64	164.69	0.076
8	40	600.5	160.33	0.101

As shown in Figure 11, Young's modulus decreases with the increase of plastic strain while the corresponding damage variable increases. According to continuum damage mechanics(CDM) [34], the initiation and growth of voids and micro-cracks during tensile tests lead to the decrease of effective bearing area, and thus cause a reduction of effective elastic modulus. In the tensile process of 25%-40%, the change of damage variable is slightly larger than that of the first 20%. Therefore, the nonlinear equation was used to fit the relationship between damage variable D and plastic strain $\varepsilon_{p,}$ and the fitting formula is shown in Eq.(8 . Besides, it should be pointed out that the young's modulus of the original is less than the commonly known value for the 316L (about 190 GPa , which might be caused by the use of non-standard specimens.

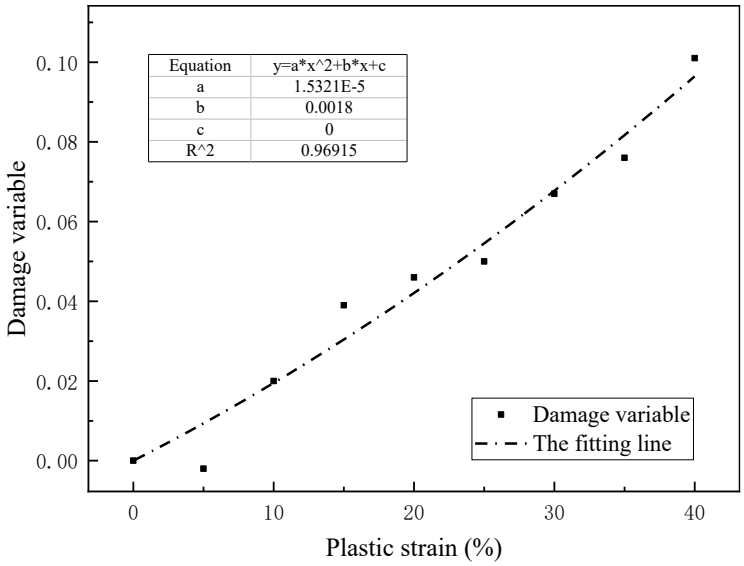

Figure 11. The variation of Young's modulus and damage variable with plastic strain

$$D = 1.532 \times 10^{-5} \varepsilon_p^2 + 0.0018 \varepsilon_p \qquad (8$$

$$D = 26.197\beta' + 2.405\sqrt{\beta' - 4.063\times10^{-4}} - 0.0059 \qquad (9$$

Combined with Eq.(6 and Eq.(8 , we correlated the relative nonlinear parameter and the damage variable of 316L specimens with the same plastic strain, and the relationship was shown in Eq.(9 . Considering the material's tensile strength, the formula is only applicable within 40% plastic deformation. Quantitative identification and evaluation of plastic damage in the failure process of the component by nonlinear ultrasonic test have a certain reference value for nondestructive testing technology to analyze metal material failure and predict the service life of equipment.

3.3 Observation of microstructures and damage evolution analysis

To study the relationship between microstructure evolution and ultrasonic nonlinearity as the plastic damage accumulation in 316L, the microstructures of the four different plastic strains (0%, 10%, 20%, and 40% were examined in this section.

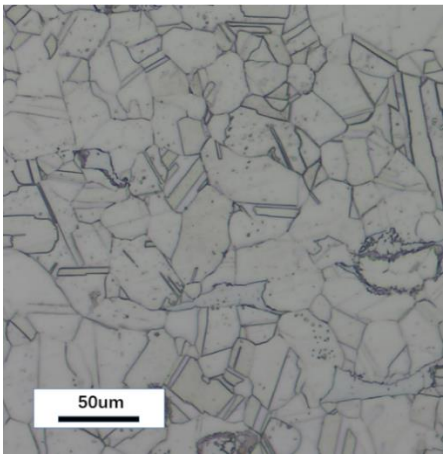

(a) initial specimen

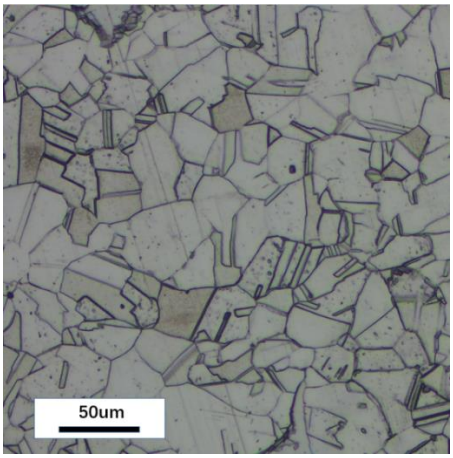

(b) 10% plastic strain

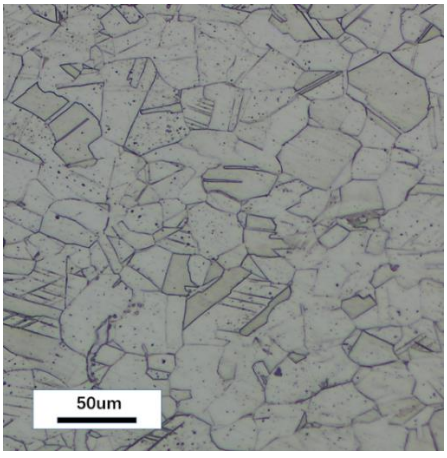

(c 20% plastic strain

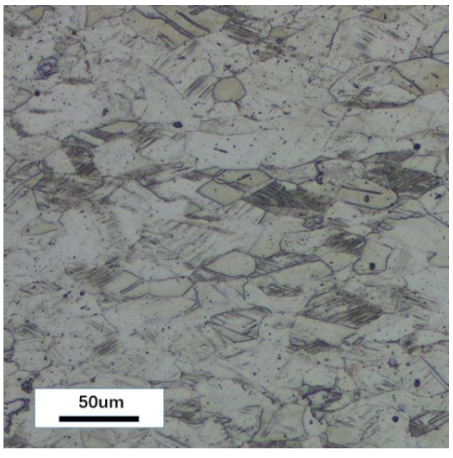

(d 40% plastic strain

Figure 12. Metallographic observation of specimens with different plastic strains

The metallographic observation, shown in Figure 12, indicates that the microstructure of the original specimen is austenite. From the sample with plastic deformation of 10%, it can be seen that the grain size is relatively small, and some grains are broken due to tensile action. In the sample with 20% plastic strain, it is observed that the grain is gradually elongated. Compared with the initial pattern, the grain size is significantly smaller, and the microstructure began to undergo phase transformation. As the deformation continues to increase, the degree of grain fragmentation

also increases. A large number of lath martensite structures can be obviously observed in the sample with plastic strain of 40%.

3.3.1 TEM observations

The representative TEM micrographs of the specimens with different plastic strains have been shown in Figure 13 which describe the evolution of dislocations during the deformation. Figure 13(a shows that only a few dislocation lines are scattered in the original specimen. The dislocation density is low, which is about $0.747\times10^{14}m^{-2}$ according to Eq.(3 . As the plastic deformation increases to 10%, the dislocation lines in the sample increase significantly, and some complex dislocation configurations such as dislocation winding begin to appear. The dislocation density calculated with Figure 13(b is about $1.78\times10^{14}m^{-2}$. For the specimens with 20% and 40% plastic strain, the winding of dislocation lines is more complex and gradually forms a cellular structure. The calculation method of dislocation density by TEM photos is no longer applicable considering the formed dislocation cells and shear band shown in Figure 13(c and (d . Therefore, based on the rheological method, this paper takes the dislocation density of the original specimen and 10% plastic strain specimen as the reference, and uses the flow stress formula (Eq.(10 to calculate the dislocation density ρ of the samples with 20% and 40% plastic strain. The calculation results are $3.11\times10^{14}m^{-2}$ 和 $4.58\times10^{14}m^{-2}$, respectively.

$$\sigma = \lambda G b_s \sqrt{\rho} \qquad (10$$

where σ is the flow stress (the value of σ is defined as 1.15 times of the average value of yield strength and tensile strength of the material， λ is a constant related to the material (0.3 ， G is the shear modulus (76 GPa ，b_s is the magnitude of the Burger vector (2.5 nm .

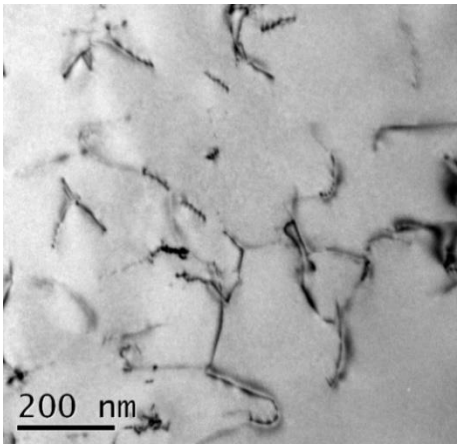

(a) initial specimen

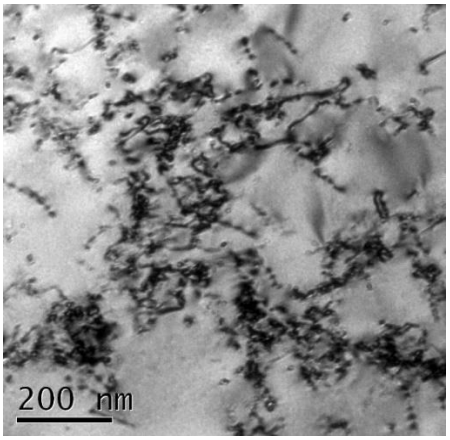

(b) 10% plastic strain

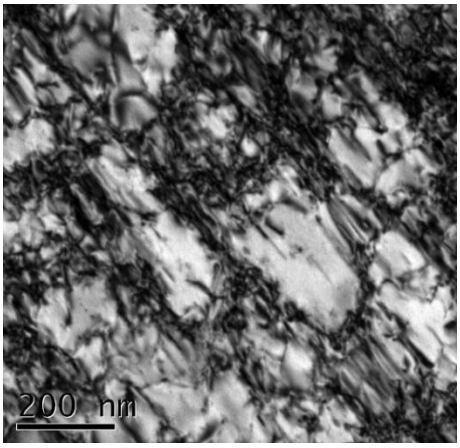

(c 20% plastic strain

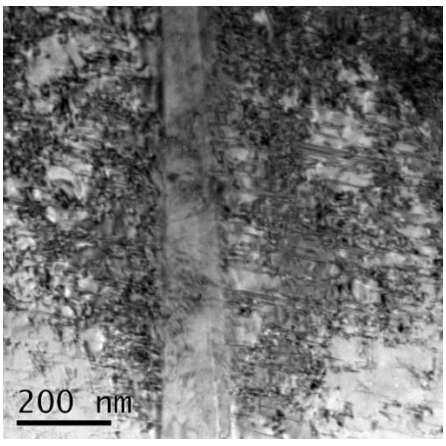

(d 40% plastic strain

Figure 13. The TEM micrographs of 316L tensile specimens with different plastic strains: (a 0%, (b 10%, (c 20%, (d

40%

3.3.2 EBSD observations

Figure 14 shows the IPF images, KAM and GROD maps observed by EBSD scan of the different plastic strains specimens. The IPF image shows the grain size of sample with 10% plastic strain became smaller, and the grains of 20% and 40% plastic strain samples showed obvious elongation and fragmentation along the loading direction. Overall, according to the qualitative analysis in Figure 14, the value of KAM and GROD increase significantly with the increase of macro plastic deformation. Due to the different orientations of individual grains in the observation area, the local deformation of crystalline materials is non-uniform. Therefore, in this paper, intergranularly averaged $\overline{\mathrm{KAM}}$ and $\overline{\mathrm{GROD}}$ are used to quantitatively characterize the deformation degree at grain scale. Figure 15 shows the evolution law of the two intragranular misorientation parameters of 316L specimens during plastic deformation. When the specimen was stretched to 10% plastic deformation, $\overline{\mathrm{KAM}}$ increased with a slow growth, while the greater plastic deformation lead to a rapid increase of the value. As for $\overline{\mathrm{GROD}}$, it is generally linear with plastic deformation. Both $\overline{\mathrm{KAM}}$ and $\overline{\mathrm{GROD}}$ establish a positive correlation with macro plastic deformation, which verifies the two-dimensional tensile model of polycrystalline materials proposed by Rui et al. [35], shown in Eq.(11) and Eq.(12). From Eq.(11), the $\overline{\mathrm{KAM}}$ values is directly correlated to the EBSD scanning step s and average geometrically necessary dislocation density $\bar{\rho}^{e}_{\mathrm{Gnd}}$. The further suggests that, the $\overline{\mathrm{KAM}}$ values can be used as an approximate measure of the real dislocation density if the step s is constant. From Eq.(12), the $\overline{\mathrm{GROD}}$ values are not affected by the above variables. Thus, the $\overline{\mathrm{GROD}}$ can be used for measuring of plastic deformation of specimen.

$$\overline{\mathrm{KAM}}=\frac{\mathrm{S_{GrainA}}\cdot\mathrm{KAM_A}+\mathrm{S_{GrainB}}\cdot\mathrm{KAM_B}+\cdots}{\mathrm{S_{GrainA}}+\mathrm{S_{GrainB}}+\cdots}=\frac{4s\zeta^{*}\varepsilon^{p}}{\pi \mathrm{D}^{*}_{\mathrm{Grian}}}=\frac{2sb_s}{\pi}\bar{\rho}^{\mathrm{e}}_{\mathrm{Gnd}} \quad (11)$$

$$\overline{\mathrm{GROD}}=\frac{\mathrm{S_{GrainA}}\cdot\mathrm{KAM_A}+\mathrm{S_{GrainB}}\cdot\mathrm{KAM_B}+\cdots}{\mathrm{S_{GrainA}}+\mathrm{S_{GrainB}}+\cdots}=\frac{2}{3}\zeta^{**}\varepsilon^{\mathrm{P}} \quad (12)$$

where ε^{P} is the macro plastic strain and $\mathrm{D}^{*}_{\mathrm{Grian}}$ is the average grain size, $\mathrm{S_{Grain\ A}}$ and $\mathrm{KAM_A}$ are area and the average misorientation of grain A，respectively. ζ^{*} and ζ^{**} are the proportionality coefficient which are independent of grain orientation.

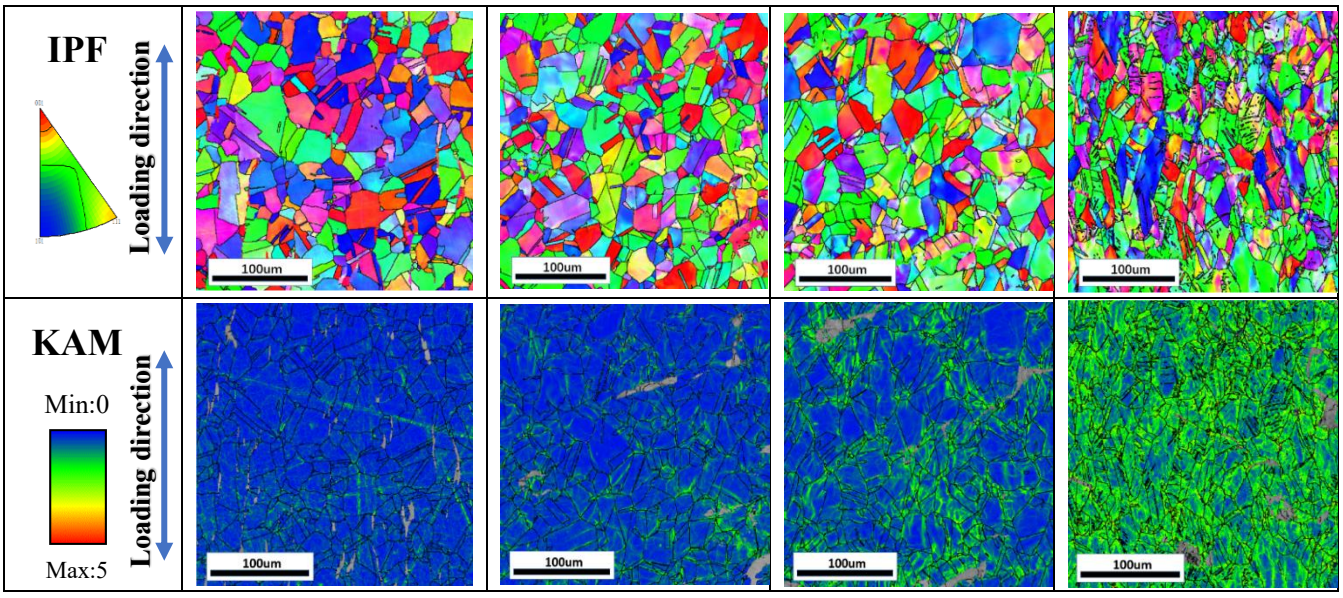

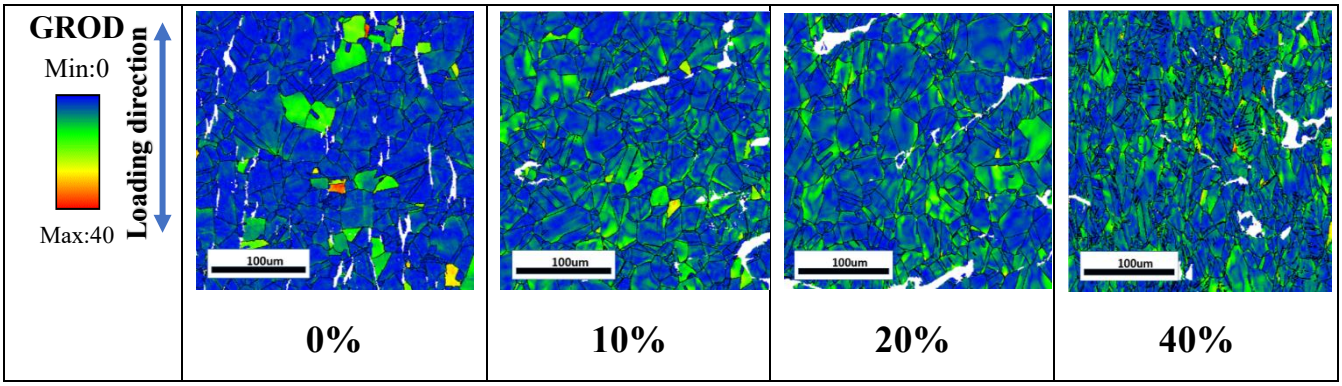

Figure 14. The IPF images, KAM and GROD maps obtained from EBSD scans of the different plastic strains specimens

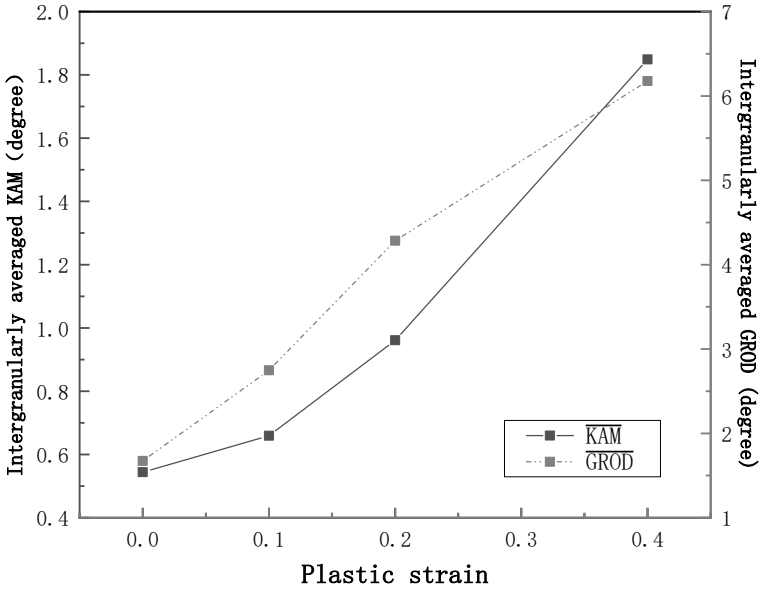

Figure 15. Variation of $\overline{\text{KAM}}$ and $\overline{\text{GROD}}$ values with the plastic strain

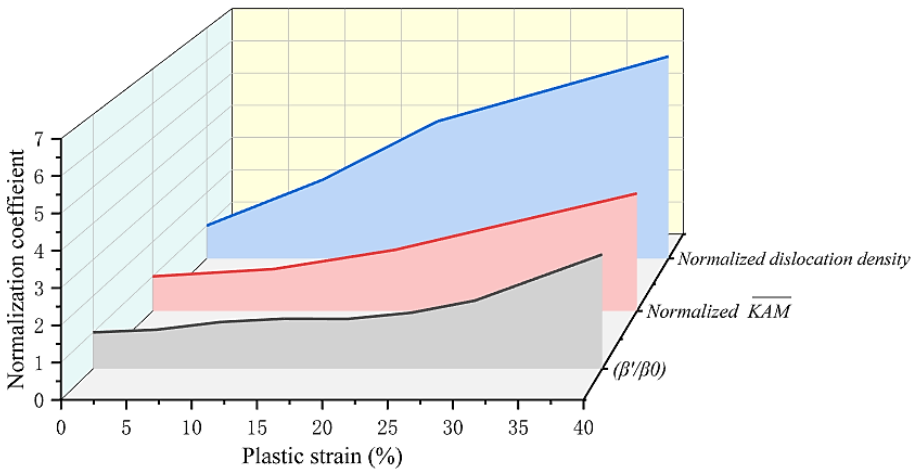

Figure 16. Comparison of variation trend of the β'/β_0, normalized $\overline{\text{KAM}}$ and normalized dislocation density with plastic strain.

To study the relationship between the evolution state of microstructure and the ultrasonic nonlinearity of 316L during the damage process, the relative nonlinear parameter β', $\overline{\mathrm{KAM}}$ and dislocation density of the sample with different plastic strain were normalized respectively, and the variation of them were plotted in Figure 16. Although it can be seen that the variation trend of dislocation density is roughly consistent with the nonlinear parameter, it should be noted the increase of nonlinear dislocation density is greater than that of the other two parameters, and the slope of the curve changes at the strain of 20%. This may be due to the different calculation methods of dislocation density between the first two samples and the latter two samples. The complex microstructure such as dislocation entanglement and phase transition cannot be performed by the method of calculating dislocation density from TEM micrograph, which leads to a smaller calculation result.

As an approximate measure of dislocation density, $\overline{\mathrm{KAM}}$ could more accurately characterize the microstructure evolution at the grain scale (including the dislocation proliferation, phase transformation etc. by obtaining the information regarding strain distribution of local grain. Figure 16 clearly shows that the variation of the normalized $\overline{\mathrm{KAM}}$ values follow the same trend as β'/β_0 basically, as well as the amplitude. Combined with the observation of microstructures, it can conclude that the damage in 316L due to tensile is controlled by the microstructure changes such as the dislocation proliferation, martensitic transformation and phase boundaries etc. which directly affects nonlinear response of materials. From the damage evolution mechanism, it further demonstrated that the nonlinear ultrasonic parameter β can accurately evaluate the plastic damage and state of microstructure evolution of 316L.

4. Conclusion

In this paper, the nonlinear ultrasonic Lamb wave was used to evaluate the tensile damage of an austenitic stainless steel 316L. The nonlinear ultrasonic response of the specimen under different plastic deformation shows the sensitivity of the nonlinear ultrasonic parameter β to the early plastic damage and mechanical degradation of metal components. By observing the microstructure evolution during the damage process, the relationship between tensile damage and ultrasonic nonlinear response is discussed. The following remarks are obtained from the investigations mentioned above.

(1) As the tensile damage of stainless steel 316L increases, the nonlinear ultrasonic parameter using Lamb wave increases monotonically. A power-law relationship between the relative nonlinear ultrasonic parameter β' and plastic strain, shown in Eq.(6 , is presented.

(2) The effects of different degrees of tensile test on the evolution of the microstructures were examined. During the tensile process, grain refinement and generation of martensitic transformation can be observed in the metallographic pictures of the material. From the TEM micrographs, it is seen that plane dislocations density increase rapidly during the initial deformation. When the plastic deformation reaches 20%, there are many complex dislocation patterns, such as dislocation winding and dislocation cell structure, and so on. $\overline{\mathrm{KAM}}$ values, as a parameter for describing the strain distribution of grains, can approximately characterized the distribution of dislocation when the scanning step s is certain. Meanwhile, the same variation trend of $\overline{\mathrm{KAM}}$ values and the normalized nonlinear parameter along with the increase of plastic strain, demonstrates the nonlinearity due to tensile damage is controlled by the evolution of microstructure that directly affects higher order elastic constant of stainless steel 316L. This proves that the tensile damage of stainless steel 316L can be evaluated by nonlinear ultrasonic parameter from the damage mechanism.

(3) Combined with the results of the cyclic tensile test, it can conclude that microstructure evolution, such as grain refinement, martensitic transformation and dislocation proliferation, are the main reasons for the increase of yield strength of 316L specimen after plastic deformation. The functional relation of damage variable D- relative nonlinear parameter β' was proposed in this study based on the CDM by fitting the experimental values of the two parameters. It is of important reference value for NDT technology to evaluate mechanical properties quantitatively and predict service life.

Acknowledgement

The authors gratefully acknowledge the supports from the National Natural Science Foundation of China (52150710540, 51905484 and 51828501 , supports provided by China Scholarship Council and the assistance of Shandong University Testing and Manufacturing Center for Advanced Materials and the University of Strathclyde.

References

[1] S.J. Zinkle, G.S. Was. Materials challenges in nuclear energy, Acta Materialia, 61 (2013 : 735-758.

[2] K.H. Lo, C.H. Shek, J.K.L. Lai. Recent developments in stainless steels, Materials Science & Engineering R-Reports, 65 (2009 : 39-104.

[3] W.H. Zhu, J.L. Rose. Lamb wave generation and reception with time-delay periodic linear arrays: A BEM simulation and experimental study, Ieee Transactions on Ultrasonics Ferroelectrics and Frequency Control, 46 (1999 : 654-664.

[4] S.S. Kessler, S.M. Spearing, C. Soutis. Damage detection in composite materials using Lamb wave methods, Smart Materials and Structures, 11 (2002 : 269-278.

[5] Y.L. Zhou, X.D. Qian, A. Birnie, X.L. Zhao. A reference free ultrasonic phased array to identify surface cracks in welded steel pipes based on transmissibility, International Journal of Pressure Vessels and Piping, 168 (2018 : 66-78.

[6] B.S. Ben, B.A. Ben, K.A. Vikram, S.H. Yang. Damage identification in composite materials using ultrasonic based Lamb wave method, Measurement, 46 (2013 : 904-912.

[7] J. Rao, M. Ratassepp, Z. Fan. Guided Wave Tomography Based on Full Waveform Inversion, Ieee Transactions on Ultrasonics Ferroelectrics and Frequency Control, 63 (2016 : 737-745.

[8] D.N. Alleyne, P. Cawley. Optimization of lamb wave inspection techniques, Ndt & E International, 25 (1992 : 11-22.

[9] L. Wang, W. Chen, X. Tan, J. Yang. The impact of various crack geometrical parameters on stress field over tip under different mixed loading conditions and inclination angles, Theoretical and Applied Fracture Mechanics, 102 (2019 : 239-254.

[10] A.K. Metya, A. Das, S. Tarafder, K. Balasubramaniam. Nonlinear Lamb wave for the evaluation of creep damage in modified 9Cr-1Mo steel, Ndt & E International, 107 (2019 .

[11] P.F. Wang, W.Q. Wang, J.F. Li. Research on Fatigue Damage of Compressor Blade Steel KMN-I Using Nonlinear Ultrasonic Testing, Shock and Vibration, 2017 (2017 .

[12] A. Hikata, B.B. Chick, C. Elbaum. Dislocation Contribution to the Second Harmonic Generation of Ultrasonic Waves, Journal of Applied Physics, 36 (1965 : 229-236.

[13] R. Truell, Ultrasonic Methods in Solid State Physics, Academic Press, 1969

[14] J. Herrmann, J.Y. Kim, L.J. Jacobs, J.M. Qu, J.W. Littles, M.F. Savage. Assessment of material damage in a nickel-base superalloy using nonlinear Rayleigh surface waves, Journal of Applied Physics, 99 (2006 .

[15] X. Wang, X. Wang, X.L. Hu, Y.B. Chi, D.M. Xiao. Damage assessment in structural steel subjected to tensile load using nonlinear and linear ultrasonic techniques, Applied Acoustics, 144 (2019 : 40-50.

[16] C. Pruell, J.Y. Kim, L.J. Jacobs, J. Qu. Generation and detection of lamb waves to detect plasticity‐induced changes in the microstructure, American Institute of Physics, 975 (2008 : 1275.

[17] A. Viswanath, B.P.C. Rao, S. Mahadevan, P. Parameswaran, T. Jayakumar, B. Raj. Nondestructive assessment of tensile properties of cold worked AISI type 304 stainless steel using nonlinear ultrasonic technique, Journal of Materials Processing Technology, 211 (2011 : 538-544.

[18] J.F. Zhang, S.Y. Li, F.Z. Xuan, F.Q. Yang. Effect of plastic deformation on nonlinear ultrasonic response of austenitic stainless steel, Materials Science and Engineering a-Structural Materials Properties Microstructure and Processing, 622 (2015 : 146-152.

[19] ASTM A959-19, Standard Guide for Specifying Harmonized Standard Grade Compositions for Wrought Stainless Steels, 2019
[20] GB/T 228.1-2010, Metallic materials-tensile testing part 1 : method of test at room temperature, Standardization Administration of the PRC, Beijing, PR China.
[21] P.F. Wang, Q.W. Zhou, B.B. Chen, S.L. Zheng, C. Wang, Z.L. Gao. Research on high cycle fatigue damage characterization of FV520B steel based on the nonlinear Lamb wave, Journal of Strain Analysis for Engineering Design.
[22] M.F. Muller, J.Y. Kim, J.M. Qu, L.J. Jacobs. Characteristics of second harmonic generation of Lamb waves in nonlinear elastic plates, Journal of the Acoustical Society of America, 127 (2010 : 2141-2152.
[23] M.S. Pham, C. Solenthaler, K.G.F. Janssens, S.R. Holdsworth. Dislocation structure evolution and its effects on cyclic deformation response of AISI 316L stainless steel, Materials Science and Engineering a-Structural Materials Properties Microstructure and Processing, 528 (2011 : 3261-3269.
[24] J. Pesicka, R. Kuzel, A. Dronhofer, G. Eggeler. The evolution of dislocation density during heat treatment and creep of tempered martensite ferritic steels, Acta Materialia, 51 (2003 : 4847-4862.
[25] J.C. Glez, J. Driver. Orientation distribution analysis in deformed grains, Journal of Applied Crystallography, 34 (2001 : 280-288.
[26] D. Kobayashi, M. Miyabe, Y. Kagiya, R. Sugiura, A.T. Yokobori. An Assessment and Estimation of the Damage Progression Behavior of IN738LC under Various Applied Stress Conditions Based on EBSD Analysis, Metallurgical and Materials Transactions a-Physical Metallurgy and Materials Science, 44A (2013 : 3123-3135.
[27] M. Kamaya. Assessment of local deformation using EBSD: Quantification of accuracy of measurement and definition of local gradient, Ultramicroscopy, 111 (2011 : 1189-1199.
[28] M. Kamaya, A.J. Wilkinson, J.M. Titchmarsh. Quantification of plastic strain of stainless steel and nickel alloy by electron backscatter diffraction, Acta Materialia, 54 (2006 : 539-548.
[29] A.J. Wilkinson, G. Meaden, D.J. Dingley. Mapping strains at the nanoscale using electron back scatter diffraction, Superlattices and Microstructures, 45 (2009 : 285-294.
[30] T. Sritharan, R.S. Chandel. Phenomena in interrupted tensile tests of heat treated aluminium alloy 6061, Acta Materialia, 45 (1997 : 3155-3161.
[31] J. Lemaitre. A CONTINUOUS DAMAGE MECHANICS MODEL FOR DUCTILE FRACTURE, Journal of Engineering Materials and Technology-Transactions of the Asme, 107 (1985 : 83-89.
[32] V. Mertinger, E. Nagy, F. Tranta, J. Solyom. Strain-induced martensitic transformation in textured austenitic stainless steels, Materials Science and Engineering a-Structural Materials Properties Microstructure and Processing, 481 (2008 : 718-722.
[33] E. Nagy, V. Mertinger, F. Tranta, J. Solyom. Deformation induced martensitic transformation in stainless steels, Materials Science and Engineering a-Structural Materials Properties Microstructure and Processing, 378 (2004 : 308-313.
[34] Lemaitre J. A Course on Damage Mechanics. Ber-lin: Springer-Verlag, 1992: 1-20.
[35] S.S. Rui, Y.B. Shang, Y.N. Fan, Q.N. Han, L.S. Niu, H.J. Shi, K. Hashimoto, N. Komai. EBSD analysis of creep deformation induced grain lattice distortion: A new method for creep damage evaluation of austenitic stainless steels, Materials Science and Engineering a-Structural Materials Properties Microstructure and Processing, 733 (2018 : 329-337.